RSC Advances

PAPER

View Article Online
View Journal | View Issue

Cite this: *RSC Adv.*, 2015, **5**, 45038

Structural and electrochemical evaluation of a TiO_2–graphene oxide based sandwich structure for lithium-ion battery anodes†

Yixing Ye,[a] Panpan Wang,[ab] Hongmei Sun,[ab] Zhenfei Tian,[a] Jun Liu[a] and Changhao Liang*[ab]

Received 26th March 2015
Accepted 12th May 2015

DOI: 10.1039/c5ra05376e

www.rsc.org/advances

In this paper, we report a rational sandwich composite structure consisting of polyaniline (PANI), amorphous TiO_2 (a-TiO_2), and a GO network as an anode material for lithium-ion batteries (LIBs). After the synthesis of the a-TiO_2–GO composite assisted by laser ablation in liquid, PANI nanorods are vertically grown on the both sides of a-TiO_2–GO nanosheets to obtain a stable sandwich structure. The morphology and components of the composites are confirmed by scanning electron microscopy, transmission electron microscopy, and Raman spectroscopy. As a typical anode material in LIBs, the fabricated sandwich composites display a high rate capability and long cycle life. A first discharge capacity of 1335 mA h g^{-1} is shown at 50 mA g^{-1} and a reversible capacity of 435 mA h g^{-1} is achieved after 250 cycles at 100 mA g^{-1}. Even at a high cycling rate of 10 A g^{-1}, the sandwich products exhibit a stable capacity of 141 mA h g^{-1}. This effort highlights the design of a sandwich structure using amorphous TiO_2, GO, and PANI nanorods and its potential benefits for LIB application.

Introduction

The development of an appropriate anode material and/or structure for lithium-ion batteries (LIBs) with high capacity, stability, and environmentally-friendly performances is always a great challenge. Among the various available candidate metal oxide anode materials, nanostructured TiO_2 has been mostly investigated as a result of its excellent safety, small volume variation (less than 4%), high rate capability, and long cycle life.[1,2] However, during discharge/charge cycles, nanoscale TiO_2 tends to agglomerate and decompose, leading to decreases in electroactive sites and fading of specific capacities.[1] Consequently, the rate of Li^+ ion insertion and extraction is slowed down and limited in TiO_2.[3] Several strategies, including design of a yolk-shell structure and minimization of diffusion distances using TiO_2 nanostructured materials, among others, have been used to address these problems.[4,5]

Besides, appropriate conductive substrates or channels for electrons movement and transport is also critical for improving LIBs performance. Graphene or reduced graphene oxide (rGO), as a two dimensional conductive network, is considered to be an ideal substrate for application in LIBs due to its superior electronic conductivity, chemical stability, and high surface area.[1,6–8] Furthermore, the structural flexibility, ample edges, and surface active sites of graphene also provide conduction channels for electron transport and allow other nanoscale materials to settle well onto the graphene network to form a composite structure.[4] As shown in the reported work, such composites with good conductive property exhibit advanced performance in electrochemical application.[9–11] Motivated by these points, we present herein a rational design to immobilize TiO_2 nanocrystals onto GO assisted *via* a laser ablation in liquid (LAL) technique. It is well known that kinds of energetic species, including atoms, molecules, electrons, ions, and clusters, are generated during laser–matter interaction confined in a liquid environment.[12] After subsequent quenching and reaction with other chemical or physical processes, these energetic species can be grown into desirable nanomaterials and structures in a tuneable manner.[13–19] In recent decades, LAL has been served as an effective route for synthesizing nanomaterials with high activity and reactivity.[12,20] Interestingly, because of no using of additional surfactant and ion sources, LAL is also recognized as a simple and green way to obtain nanomaterials with clean surfaces, small sizes, and abundant defects.[20] LAL-generated nanomaterials with high activity have been proven to show good performance in electric and photocatalytic applications, even at small quantities.[19,21–23]

In our previous work, graphene was demonstrated to be a potential substrate for capturing the energetic species produced

[a]*Key Laboratory of Materials Physics and Anhui Key Laboratory of Nanomaterials and Nanotechnology, Institute of Solid State Physics, Hefei Institutes of Physical Science, Chinese Academy of Sciences, Hefei 230031, China. E-mail: chliang@issp.ac.cn*

[b]*University of Science and Technology of China, Hefei 230026, China*

† Electronic supplementary information (ESI) available: Assembled two-electrode CR2032-type coin cells, TEM images of GO, SEM images of as-prepared products, contrast of first discharge capacity of PANI/a-TiO_2–GO/PANI at 50 mA g^{-1} and 100 mA g^{-1}. See DOI: 10.1039/c5ra05376e

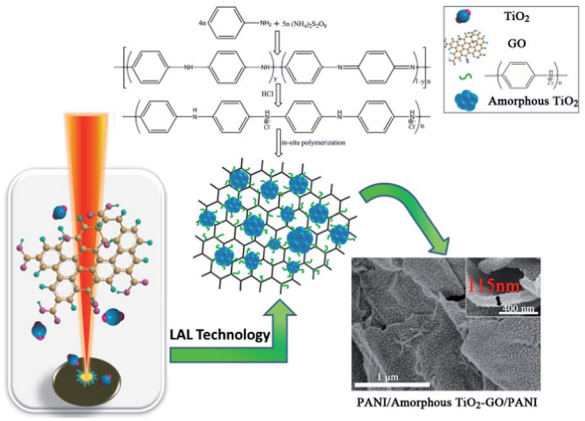

Scheme 1 Design of the PANI/amorphous TiO_2–GO/PANI sandwich structure.

by LAL in colloidal solutions.[23] Strong interactions between active species and GO, which is rich in surface groups, allow the formation of well-dispersed nanoparticles throughout the GO network in a simple solution way. As shown in Scheme 1, GO was first employed in active colloid to catch LAL-generated TiO_2 nanoparticles. Specifically, in our design, the LAL-generated TiO_2 was characterized to be amorphous, which has been reported to show advanced performance in LIBs application.[4,24,25] Further, polyaniline (PANI), a typical conducting polymer,[26–30] was used as a promising shell material in our design and grown on the both sides of amorphous-TiO_2–GO (a-TiO_2–GO) nanocomposite to obtain a stable sandwich structure. Use of this sandwich nanostructure as an anode material in LIBs resulted in a first discharge capacity of 1335 mA h g^{-1} at 50 mA g^{-1} and a reversible capacity of 435 mA h g^{-1} at 0.1 A g^{-1} after 250 cycles. The sandwich structure even exhibited a stable capacity of 141 mA h g^{-1} at a high cycling rate of 10 A g^{-1}. This effort highlights the design of a sandwich structure by using amorphous TiO_2, GO, and PANI nanorods and promises its potential benefits for LIBs application.

Experimental section

Chemical reagents and materials

Graphite powder (AR) was purchased from Tianjin Guangfu Fine Chemical Research Institute. Hydrochloric acid (HCl) and aniline were purchased from Sinopharm Chemical Reagent Co., Ltd. Ammonium persulfate (APS) was obtained from Tianjin Bodi Chemical Co., Ltd. All reagents used in this experiment were of analytical grade and applied without further purification.

Formation of PANI/amorphous TiO_2–GO/PANI sandwich composite

GO was synthesized from a modified Hummers method.[31,32] Typically, for the fabrication of sandwich PANI/amorphous TiO_2–GO/PANI nanocomposite (PANI/a-TiO_2–GO/PANI), 600 μL of HCl was firstly added into 40 mL of GO aqueous solution with an ice bath, and the mixture was stirred until GO and HCl fully dispersed. Afterward, a TiO_2 plate (purity, 99.99%) was fixed in a vessel filled with the mixture solution described above; the metal oxide plate was then ablated for 30 min in a rotating state by a fundamental (1064 nm) Nd:YAG laser with 10 Hz pulse repetition rate, 6 ns pulse duration, and 100 mJ pulse energy density. A dark brown colloidal solution was obtained after ablation. Then the aniline monomer was added into the above colloidal solution, and stirred for 30 min in an ice bath to produce a uniform mixture. The oxidant powder, $(NH_4)_2S_2O_8$ (APS), was added into the above solution under rapid agitation (molar ratio of aniline/APS, 1.5). After 24 h, the result green product (Fig. S1, in ESI†) was collected by centrifugation and dried at 50 °C for 24 h in a vacuum chamber. For comparison, PANI/GO/PANI was also synthesized without TiO_2 colloid in the same way.

Structure and morphology characterization

The typical morphology and structure of the composite were investigated by scanning electron microscopy (SEM, Sirion 200 FEG) and transmission electron microscopy (TEM, JEOL-2010 with 200 kV accelerating voltage). Specimens for TEM were prepared as follows: a small amount of powder was dispersed in ethanol to form a uniform suspension that was then dropped onto a carbon-coated Cu grid. The functional group information of the as-prepared composite was determined by Raman spectroscopy using an SPEX-1403 laser Raman spectrometer with a 514.5 nm Ar^+ laser excitation. X-ray diffraction (XRD) analysis of the collected powder products was performed by using a Philips X'Pert system with Cu-Ka radiation ($\lambda = 1.5419$ Å).

Electrochemical measurement

The PANI/a-TiO_2–GO/PANI composite powder was mixed with Super P and sodium carboxymethyl cellulose at a weight ratio of 80 : 10 : 10 to produce electrode slurry. The electrochemical performance of as-fabricated working electrode was investigated by a two-electrode CR2032-type coin cells (Fig. S1 in ESI†), in which metallic lithium foil was used as the counter electrode, and porous polypropylene films was used as separator; the electrolyte was 1 M LiPF6/EC and DEC (1 : 1 by volume ratio; ethylene carbonate (EC) and diethyl carbonate (DEC) was purchased from Zhuhai Smoothway Electronic Materials Co., Ltd.). Discharge/charge testing was conducted at various rates within the voltage window from 0.01 V to 3.0 V (*vs.* Li^+/Li) on an LANHE battery testing system (Wuhan, China). Electrical impedance spectroscopy (EIS) experiments were carried out on a Zahner electrochemical workstation (Zennium, Germany) in the frequency range from 100 kHz to 10 mHz with an AC signal amplitude of 5 mV. Cyclic voltammetry (CV) experiments were performed on the same workstation in the voltages ranging from 0.01 V to 3 V.

Results and discussion

Aqueous GO solution was produced from natural flaked graphite *via* modified Hummers method,[31,32] in which GO exists as a single- or few-layer structure (Fig. S2†). In the absence of

GO, the products exhibit a morphology of long wires with a diameter of about 50 nm as shown in Fig. S3a.† GO with a considerable number of oxygen-containing groups can provide a large amount of growth sites for PANI,[33] and PANI nanorods can be grown on GO with a sandwich structure of 100 nm thickness (Fig. S3b†). In our case, the a-TiO_2–GO composite was prepared by ablating a TiO_2 plate in aqueous GO solution with HCl. Fresh LAL-generated colloidal nanoparticles have been mostly proven to exhibit high activity and an abundance of defects.[12] These defects and active sites on a-TiO_2–GO nanosheet prefer to minimize the interfacial energy barrier between the solid surface and bulk solution, and are impactful for the subsequent growth of PANI nanorods.[33] When aniline is introduced, these defects and active nucleation sites are utilized on the surfaces of a-TiO_2–GO at the beginning of the polymerization process by heterogeneous nucleation.[33] Fig. S3c† shows the curly layer morphology of obtained PANI/a-TiO_2–GO/PANI composite; here, PANI nanorods are vertically aligned on both sides of the a-TiO_2–GO layer. The thickness of result sandwich structure reaches 115 nm, as shown in the bottom right corner of Scheme 1.

In addition, XRD analysis of TiO_2–GO did not show obvious diffraction peaks of crystalline TiO_2, which is corresponded with the disorder internal structure of TiO_2 shown in the inset TEM image in Fig. 1a. And these investigations revealed the amorphous-like nature of TiO_2 nanoparticles. Fig. 1b shows a typical TEM image of the a-TiO_2–GO composite layer. LAL-generated TiO_2 particles with sizes of around 50 nm were dispersed onto the GO nanosheets *in situ*. The fresh a-TiO_2–GO solution was used as a substrate for growing PANI nanorods. PANI can act as a "true" metal because of its oxidation and protonation state among conjugated polymers.[30,34–36] In the present work, HCl existing in the GO precursor solution prominently acted as a doping agent for PANI protonation. The left image in Fig. 1c shows the mapping elemental images of C, Cl, Ti, and O; elemental Cl was homodispersed in the as-prepared PANI/a-TiO_2–GO/PANI composite, and this finding suggests the superior conductivity of PANI.[29,35,36] After covering with PANI nanorods, the final TiO_2 nanoparticles are still exhibited to be amorphous in SAED and TEM images on the right-hand side of Fig. 1c.

Raman measurements were carried out to verify the existence of PANI in PANI/a-TiO_2–GO/PANI sandwich structure, as shown in Fig. 2. The red, black, and green lines correspond to the TiO_2 colloid, a-TiO_2–GO, and PANI/a-TiO_2–GO/PANI in the sandwich structure, respectively. Compared with the TiO_2 colloid and a-TiO_2–GO, the Raman spectrum of the sandwich structure displayed two additional shoulder peaks located at 1175.8 and 1465.3 cm^{-1} except for the typical Raman features of GO with the presence of D and G bands. As reported in previous works,[27,37,38] the two additional peaks correspond to C–H vibrations in the quinoid/phenyl groups and the semiquinone radical cation structure in molecular PANI, respectively. The peak at 813 cm^{-1} was assigned to C–N–C wag out-of-plane vibrations of the benzenoid ring in the EM salt state.[37] SEM, TEM, and Raman measurements clearly demonstrated the successful synthesis of the PANI/a-TiO_2–GO/PANI sandwich composite structure.

Well-ordered nanostructure can reduce the ionic diffusion path, facilitate ionic motion to the inner part of result products, and improve the utilization of electrode materials.[33] To probe the potential battery application of the as-prepared sandwich structure, the samples were assembled as electrodes for LIBs with performances shown in Fig. 3 and S4.† At 50 mA g^{-1}, the first discharge capacity of PANI/a-TiO_2–GO/PANI was achieved to be about 1335 mA h g^{-1} and shown a plateau at ~1.5 V (Fig. S4†). Moreover, the first discharge/charge capacity of PANI/a-TiO_2–GO/PANI exhibited to be 591/300 mA h g^{-1} at 100 mA g^{-1} (Fig. 3a); a plateau at ~1.5 V was also observed in the first discharge curve, which can be confirmed by CV measurements in Fig. 3b. The relatively low columbic efficiency in the first cycle is usually attributed to the existence of irreversible Li trapped sites and traces of adsorbed water.[29] Compared with the discharge/charge capacity of 335/291 mA h g^{-1} in the second curve, the sandwich structure exhibited a much higher stabilized discharge/charge capacity of 444/436 mA h g^{-1} at 100 mA g^{-1} even after 250 cycles (Fig. 3a and c). This rising tendency could be observed clearly in the first 50 cycles in

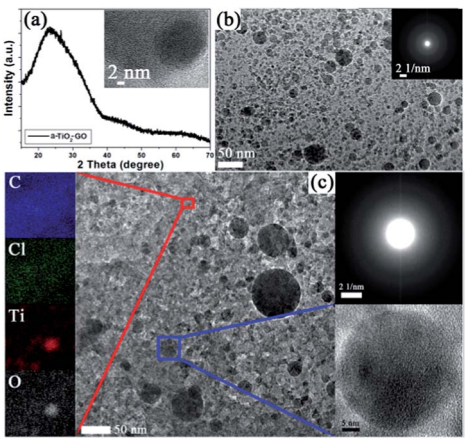

Fig. 1 (a) The XRD phase characterization of a-TiO_2–GO, (b) TEM images of a-TiO_2–GO, (c) TEM images of PANI/a-TiO_2–GO/PANI.

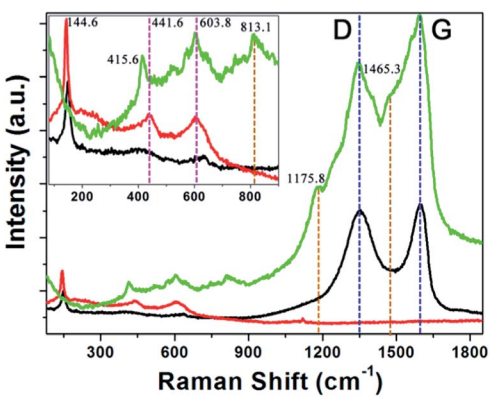

Fig. 2 Raman spectra of the TiO_2 colloid (red line), a-TiO_2–GO (black line), and PANI/a-TiO_2–GO/PANI with a sandwich structure (green line).

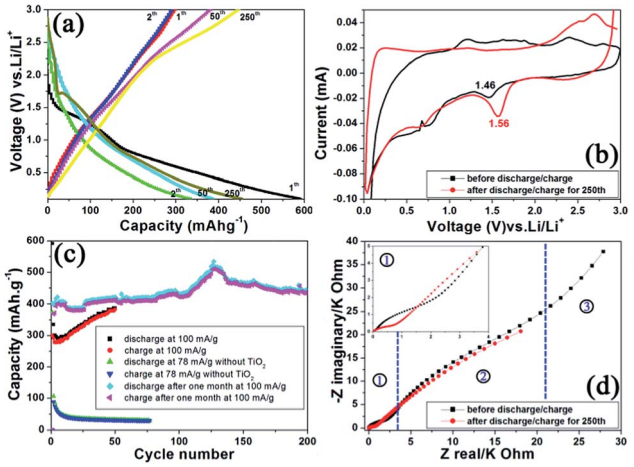

Fig. 3 Electrochemical properties of the sandwich PANI/a-TiO_2–GO/PANI nanocomposite: (a) discharge/charge capacity; (b) CV measurements; (c) cycle stability; (d) EIS measurements.

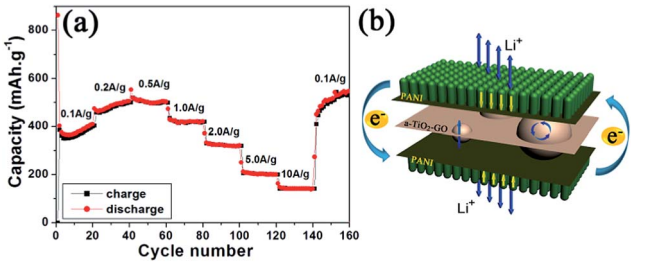

Fig. 4 (a) The stability of the sandwich PANI/a-TiO_2–GO/PANI nanocomposite by changing current densities, (b) the illustration for the transmission of Li^+ ion and e^- in the sandwich structure.

Fig. 3c. To determine the possible influencing factors for the rising of discharge/charge capacity, EIS was performed in Fig. 3d; this technique is commonly used to reflect the electron and ion transmission way of assembled electrodes. Before discharge/charge measurements, an EIS pattern typical of a Li-ion cell was exhibited (black line in Fig. 3d) by the PANI/a-TiO_2–GO/PANI structure, which is consisted of two partially overlapped semicircles and a straight sloping line at the low frequency end.[39] As previously reported, section 1 at high frequencies corresponds to the resistance of the solid-state interface layer (SEI films) formed on the surface of the electrodes. Section 2 at medium frequencies is related to the faradic charge-transfer resistance and its relative double-layer capacitance, which reflects the kinetics of the cell reaction and correlates with the apparent diffusivity of Li^+ ion in the electrodes.[39] After discharge/charge for 250 cycles (red line in Fig. 3d), the EIS shows only one semicircle and a straight sloping line. This result reveals not only the successful formation of an SEI film in the initial cycles but also a much smaller faradic charge-transfer resistance for our sandwich structure. Therefore, after several cycles, the diffusivity of Li^+ ions increased and gradually stabilized. It was considered that the forming of SEI film could not be provided with enough Li^+ ion at the initial cycles because of the different diffusivity of Li^+ ions in PANI and TiO_2. Namely, the discharge/charge capacity tended to relatively stabilized after 50 cycles in Fig. 3c. Contrasting sharply with the previous samples, the PANI/GO/PANI nanocomposite showed a lower discharge/charge capacity of 373/88 mA h g^{-1} at the first cycle in Fig. 3c. Introduction of PANI favoured the stability of the electrode structure stable as seen in Fig. 3c.[29] Moreover, as seen in the discharge and CV curve obtained at 250 cycles (Fig. 3a and b), a plateau at ~1.56 V occurs, which corresponds to a state with richer Li^+ ions than that at ~1.5 V.[5,40–42]

Fig. 4a shows the variation in discharge/charge capacity of the resultant PANI/a-TiO_2–GO/PANI with the number of cycles at different current densities. The high-rate capability and cycle stability of the sandwich structure was revealed. The discharge capacity exhibited a rising trend in the first 40 cycles as described above. At lower current densities of 0.1, 0.2, and 0.5 A g^{-1}, the discharge capacity was within 503 mA h g^{-1}. Interestingly, when the current density was increased to 10 A g^{-1}, the sandwich structure still showed a discharge capacity of 141 mA h g^{-1} after 140 cycles. More importantly, after 160 cycles at varied current densities, the discharge capacity, at 547 mA h g^{-1} (current density, 0.1 A g^{-1}), was almost identical to that at the first 40 cycles. Therefore, the sandwich structure can endure great changes in current density to retain good stability upon cycling.

The as-prepared sandwich structure exhibits a long-cycle life and high-rate capability as an anode material for LIBs application. As shown in Fig. 4b, it can be attributed to following reasons: (1) the sandwich structure of the products. Firstly, the rod-like PANI array on the both side of a-TiO_2–GO composite not only provides the fast electron conducting pathways to improve the poor electrical conductivity of a-TiO_2, but also increases the electrode/electrolyte contact area and provides extra active sites for the storage of Li^+ ion, which is able to enhance the specific capacity and high-rate capabilities. Secondly, the PANI shows features of chemical stability, good cyclability (more than 500 cycles), tunable properties, high coulombic efficiency, simple synthesis and low cost in electrode material application,[26] and hence which is beneficial for improving the cycling performance. (2) The addition of GO. GO, as a substrate to capture the active a-TiO_2 nanoparticle in fresh LAL-colloid, can prevent the aggregation of these active a-TiO_2 nanoparticles, which is critically important for the cycling stability. Moreover, GO can provide an elastic butter space to accommodate the volume change of the a-TiO_2 during the charge/discharge cycling. In addition, as seen in Fig. 2, the ratio of *I*(D peak) to *I*(G peak) of PANI/a-TiO_2–GO/PANI is smaller than that of a-TiO_2–GO, indicating that GO in PANI/a-TiO_2–GO/PANI is reduced to some extent, leading to higher electrical conductivity. (3) The TiO_2 nanoparticles obtained in this structure is demonstrated to be amorphous. And the disordered internal structure provides more channels for Li^+ ion and e^- transmission (Fig. 4b). Different from other available candidate metal oxide anode materials, TiO_2 with improved electronic conductivity has been proposed as a promising anode due to its stable structure, good safety, environmental-friendly and fast discharge/charge kinetics.[43] Besides, the presence of TiO_2

nanoparticles can prevent the restacking of GO into thick plates during repetitive cycling, and ensures the stability of the result structure from another point of view.

Conclusions

In summary, we successfully designed a sandwich composite (PANI/a-TiO_2–GO/PANI) with a high-rate capability and long cycle life as an anode material for LIBs application. The first discharge/charge capacity of PANI/a-TiO_2–GO/PANI at 100 mA g^{-1} was detected to be 591/300 mA h g^{-1}. Undergoing 250 cycles later, the sandwich composite still exhibited a stable discharge/charge capacity of 444/436 mA h g^{-1}. Moreover, the discharge capacity of the composites even displayed to be 547 mA h g^{-1} at 100 mA g^{-1} after 160 cycles at varied current densities (0.1, 0.2, 0.5, 1, 2, 5, and 10 A g^{-1}). Such a design was realized without using any surfactant or high-temperature treatment. This work provides an alternative basis for further explorations of highly efficient sandwich structures with other metal oxides for energy storage.

Acknowledgements

This work was financially supported by the National Basic Research Program of China (2014CB931704), the National Natural Science Foundation of China (NSFC, no. 11174287, 51371166, 11204308) and the CAS/SAFEA International Partnership Program for Creative Research Teams.

Notes and references

1 M. M. Zhen, X. J. Guo, G. D. Gao, Z. Zhou and L. Liu, *Chem. Commun.*, 2014, **50**, 11915–11918.
2 G. N. Zhu, Y. G. Wang and Y. Y. Xia, *Energy Environ. Sci.*, 2012, **5**, 6652–6667.
3 M. P. Cantiio, J. I. Cisneros and R. M. Torresi, *J. Phys. Chem.*, 1994, **98**, 4865–4869.
4 C. M. Ban, M. Xie, X. Sun, J. J. Travis, G. K. Wang, H. T. Sun, A. C. Dillon, J. Lian and S. M. George, *Nanotechnology*, 2013, **24**, 424002 (6pp).
5 X. B. Wang, Y. Y. Wang, L. Yang, K. Wang, X. D. Lou and B. B. Cai, *J. Power Sources*, 2014, **262**, 72–78.
6 T. B. Lan, Y. B. Liu, J. Dou, Z. S. Hong and M. D. Wei, *J. Mater. Chem. A*, 2014, **2**, 1102–1106.
7 R. W. Mo, Z. Y. Lei, K. N. Sun and D. Rooney, *Adv. Mater.*, 2014, **26**, 2084–2088.
8 W. Li, F. Wang, S. S. Feng, J. X. Wang, Z. K. Sun, B. Li, Y. H. Li, J. P. Yang, A. A. Elzatahry, Y. Y. Xia and D. Y. Zhao, *J. Am. Chem. Soc.*, 2013, **135**, 18300–18303.
9 F. Zhang, H. Q. Cao, D. M. Yue, J. X. Zhang and M. Z. Qu, *Inorg. Chem.*, 2012, **51**, 9544–9551.
10 G. P. Xiong, K. P. S. S. Hembram, R. G. Reifenberger and T. S. Fisher, *J. Power Sources*, 2013, **227**, 254–259.
11 G. P. Xiong, C. Z. Meng, R. G. Reifenberger, P. P. Irazoqui and T. S. Fisher, *Adv. Energy Mater.*, 2014, **4**, 1300515.
12 H. B. Zeng, X. W. Du, S. C. Singh, S. A. Kulinich, S. K. Yang, J. P. He and W. P. Cai, *Adv. Funct. Mater.*, 2012, **22**, 1333–1353.
13 B. H. Lee, T. Nakayama, Y. Tokoi, T. Suzuki and K. Niihara, *J. Alloys Compd.*, 2011, **509**, 1231–1235.
14 H. M. Zhang, C. H. Liang, Z. F. Tian, G. Z. Wang and W. P. Cai, *J. Phys. Chem. C*, 2010, **114**, 12524–12528.
15 D. W. Liang, S. L. Wu, P. P. Wang, Y. Y. Cai, Z. F. Tian, J. Liu and C. H. Liang, *RSC Adv.*, 2014, **4**, 26201–26206.
16 H. M. Zhang, C. H. Liang, J. Liu, Z. F. Tian and G. S. Shao, *Carbon*, 2013, **55**, 108–115.
17 Y. Ishikawa, K. Kawaguchi, Y. Shimizu, T. Sasaki and N. Koshizaki, *Chem. Phys. Lett.*, 2006, **428**, 426–429.
18 Q. Li, C. H. Liang, Z. F. Tian, J. Zhang, H. M. Zhang and W. P. Cai, *CrystEngComm*, 2012, **14**, 3236–3240.
19 J. Liu, C. H. Liang, G. P. Xu, Z. F. Tian, G. S. Shao and L. D. Zhang, *Nano Energy*, 2013, **2**, 328–336.
20 G. W. Yang, *Prog. Mater. Sci.*, 2007, **52**, 648–698.
21 C. H. Liang, Z. F. Tian, T. Tsuruoka, W. P. Cai and N. Koshizaki, *J. Photochem. Photobiol., A*, 2011, **224**, 110–115.
22 M. K. Singh, M. C. Mathpal and A. Agarwal, *Chem. Phys. Lett.*, 2012, **536**, 87–91.
23 Y. X. Ye, P. P. Wang, E. M. Dai, J. Liu, Z. F. Tian, C. H. Liang and G. S. Shao, *Phys. Chem. Chem. Phys.*, 2014, **16**, 8801–8807.
24 H. Xiong, M. D. Slater, M. Balasubramanian, C. S. Johnson and T. Rajh, *J. Phys. Chem. Lett.*, 2011, **2**, 2560–2565.
25 H. T. Fang, M. Liu, D. W. Wang, T. Sun, D. S. Guan, F. Li, J. G. Zhou, T. K. Sham and H. M. Cheng, *Nanotechnology*, 2009, **20**, 225701.
26 L. Shao, J. W. Jeon and J. L. Lutkenhaus, *Chem. Mater.*, 2012, **24**, 181–189.
27 Z. Li, H. Zhang, Q. Liu, Y. Liu, L. Stanciu and J. Xie, *ACS Appl. Mater. Interfaces*, 2014, **6**, 5996–6002.
28 H. X. Yang, T. Song, L. Liu, A. Devadoss, F. Xia, H. Han, H. Park, W. Sigmund, K. Kwon and U. Paik, *J. Phys. Chem. C*, 2013, **117**, 17376–17381.
29 C. Lai, H. Z. Zhang, G. R. Li and X. P. Gao, *J. Power Sources*, 2011, **196**, 4735–4740.
30 Q. Lu, Q. Zhao, H. M. Zhang, J. Li, X. H. Wang and F. S. Wang, *ACS Macro Lett.*, 2013, **2**, 92–95.
31 W. S. Hummers JR and R. E. Offeman, *J. Am. Chem. Soc.*, 1958, **80**, 1339.
32 Y. X. Xu, H. Bai, G. W. Lu, C. Li and G. Q. Shi, *J. Am. Chem. Soc.*, 2008, **130**, 5856–5857.
33 J. J. Xu, K. Wang, S. Z. Zu, B. H. Han and Z. X. Wei, *ACS Nano*, 2010, **4**, 5019–5026.
34 L. J. Pan, L. Pu, Y. Shi, S. Y. Song, Z. Xu, R. Zhang and Y. D. Zheng, *Adv. Mater.*, 2007, **19**, 461–464.
35 H. Cheng and S. P. Wang, *J. Mater. Chem. A*, 2014, **2**, 13783–13794.
36 H. L. Wang, Q. L. Hao, X. J. Yang, L. D. Lu and X. Wang, *Electrochem. Commun.*, 2009, **11**, 1158–1161.
37 L. Wang, Y. J. Ye, X. P. Lu, Z. B. Wen, Z. Li, H. Q. Hou and Y. H. Song, *Sci. Rep.*, 2013, **3**, 3568.
38 C. Vallés, P. Jiménez, E. Muñoz, A. M. Benito and W. K. Maser, *J. Phys. Chem. C*, 2011, **115**, 10468–10474.

39 S. S. Zhang, K. Xu and T. R. Jow, *Electrochim. Acta*, 2004, **49**, 1057–1061.
40 H. S. Kim, S. H. Yu, Y. E. Sung and S. H. Kang, *J. Alloys Compd.*, 2014, **597**, 275–281.
41 Q. H. Tian, Z. X. Zhang, L. Yang and S. Hirano, *J. Power Sources*, 2014, **253**, 9–16.
42 B. C. Qiu, M. Y. Xing and J. L. Zhang, *J. Am. Chem. Soc.*, 2014, **136**, 5852–5855.
43 W. W. Sun and Y. Wang, *Nanoscale*, 2014, **6**, 11528–11552.